Materials & Design 219 (2022) 110747

Contents lists available at ScienceDirect

Materials & Design

journal homepage: www.elsevier.com/locate/matdes

Conformable and robust microfluidic force sensors to enable precision joint replacement surgery

Liam Ives [a], Alizée Pace [a], Fabian Bor [a], Qingshen Jing [a], Tom Wade [a], Jehangir Cama [b,c,d,*], Vikas Khanduja [e,*], Sohini Kar-Narayan [a,*]

[a] Department of Materials Science and Metallurgy, University of Cambridge, 27 Charles Babbage Road, Cambridge CB3 0FS, UK
[b] Cavendish Laboratory, Department of Physics, University of Cambridge, JJ Thomson Avenue, Cambridge CB3 0HE, UK
[c] Living Systems Institute, University of Exeter, Stocker Road, Exeter EX4 4QD, UK
[d] College of Engineering, Mathematics and Physical Sciences, Harrison Building, University of Exeter, North Park Road, Exeter EX4 4QF, UK
[e] Cambridge Young Adult Hip Service, Addenbrooke's, Cambridge University Hospitals, Box 37, Hills Road, Cambridge CB2 0QQ, UK

HIGHLIGHTS

- Additively manufactured conformable microfluidic force sensor to measure forces during joint replacement.
- Quantitative force data from sensors could aid precise implant positioning and balance.
- Sensor design optimised using finite element modelling and calibrated within a 3D printed model hip implant.
- High sensitivity demonstrated at typical forces experienced during hip replacements.
- Powerful new surgical tool to aid implant positioning, increasing the lifetime of hip replacements.

GRAPHICAL ABSTRACT

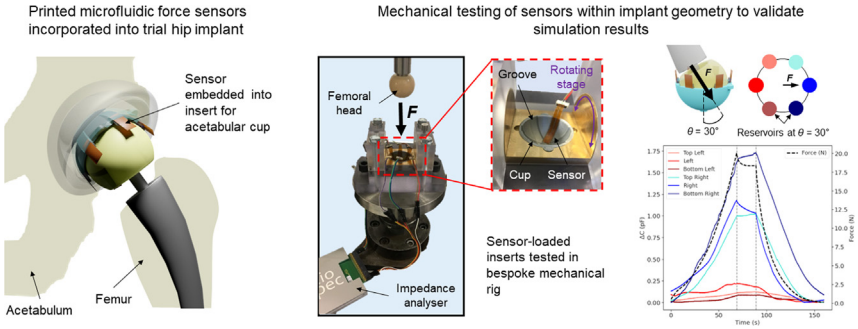

ARTICLE INFO

Article history:
Received 3 November 2021
Revised 4 May 2022
Accepted 9 May 2022
Available online 16 May 2022

Keywords:
Microfluidics
Force sensor
Total hip replacement
Additive manufacturing
Orthopaedic surgery

ABSTRACT

Balancing forces within weight-bearing joints such as the hip during joint replacement is essential for implant longevity. Minimising implant failure and the corresponding need for expensive and difficult revision surgery is vital to both improve the quality of life of the patient and lighten the burden on over-stretched healthcare systems. However, balancing forces during total hip replacements is currently subjective and entirely dependent on surgical skill, as there are no sensors currently on the market that are capable of providing quantitative force feedback within the small and complex geometry of the hip joint. Here, we solve this unmet clinical need by presenting a thin and conformable microfluidic force sensor, which is compatible with the standard surgical procedure. The sensors are fabricated via additive manufacturing, using a combination of 3D and aerosol-jet printing. We optimised the design using finite element modelling, then incorporated and calibrated our sensors in a 3D printed model hip implant. Using a bespoke testing rig, we demonstrated high sensitivity at typical forces experienced following

* Corresponding authors at: Department of Materials Science and Metallurgy, University of Cambridge, 27 Charles Babbage Road, Cambridge CB3 0FS, UK (S. Kar-Narayan); Cambridge Young Adult Hip Service, Addenbrooke's, Cambridge University Hospitals, Hills Road, Cambridge CB2 0QQ, UK (V.Khanduja).
E-mail addresses: j.cama@exeter.ac.uk (J. Cama), vk279@cam.ac.uk (V. Khanduja), sk568@cam.ac.uk (S. Kar-Narayan).

https://doi.org/10.1016/j.matdes.2022.110747

implantation of hip replacements. We anticipate that these sensors will aid soft tissue balancing and implant positioning, thereby increasing the longevity of hip replacements. These sensors thus represent a powerful new surgical tool for a range of orthopaedic procedures where balancing forces is crucial.

1. Introduction

Over 1.9 million total hip replacements (THRs) and 1.5 million total knee replacements (TKRs) were performed in the United Kingdom between April 2003 and December 2019 [1]. This rate is ever increasing, with over 280,000 THRs and 320,000 TKRs performed between 2017 and 2019. In the United States, the demands for hip and knee replacements are predicted to rise to 1,429,000 and 3,416,000 annual cases respectively by 2040 [2]. This is due to both an ageing global population and joint replacement patients being younger and more physically active than a few decades ago [2,3]. The greater the number of joint replacements, the greater the number of resultant revision procedures required when the primary implant fails. Overall, 10% of primary THRs between April 2003 and December 2019 have required revision [1], but the failure rate increases to 42% 25 years after primary hip surgery [4]. Revision surgery is expensive and technically challenging, so there is considerable interest in improving surgical procedures to maximise the implant longevity [5–11]. Implant survival or longevity is based on several factors, but implant positioning plays a fundamental role. Poor implant positioning has also been correlated with a higher rate of dislocation, prosthetic impingement, leg length inequality, implant loosening, accelerated wear and poor functional outcomes [12–14]. These comprise about 40% of the causes of revision surgery [15]. The primary THR dislocation rate is approximately 7%, whereas this rate increases to 28% for revision THRs [1]. Restoration of normal hip anatomy at the THR provides for better clinical function and abductor strength as well as reduced wear of the polyethylene implant component which is prone to failure [16–20].

The hip is a ball and socket joint, and the biomechanical goals of a total hip replacement are to achieve the correct centre of rotation of the femoral head, and accurate leg length, offset and positioning of the femoral and acetabular components, allowing hip stability. During a total hip replacement, the surgeon has access to the both the acetabulum, i.e. the socket (cup) shaped part of the pelvic bone, and the femoral head, i.e. the top of the thigh bone (the femur). After removing the damaged cartilage and bone, the acetabular part of the implant, a metal or polyethylene cup, is inserted into the acetabulum. For a metal cup, an ultra-high molecular weight polyethylene (UHMWPE) cup is inserted, to provide a low-friction articulating surface to contact the implant's femoral head. A metallic stem is inserted into the hollowed-out femur. A trial femoral head is attached to the top of the stem, and together the femoral and acetabular components are connected. The cup, head and stem components come in a range of sizes, so the implant size can be tailored to the patient's joint. The surgeon then assesses the position, stability, leg-length and soft tissue balance of the trial components by checking for combined anteversion, moving the hip through a full range of movement but especially into flexion, internal rotation, extension, external rotation and telescoping the joint. Implant repositioning and resizing are performed if required and the process of trialling is repeated. Once the trial implants are deemed to have been correctly positioned with the correct soft tissue tensioning, the trial implants are exchanged with the final implants.

It is during this trial stage that surgeons lack objective force data to aid precise positioning and balance. Quantitative force feedback could provide information on whether the cup and stem are the correct distance apart (the correct offset) which leads to accurate soft tissue balance and also whether this offers maximum stability to the joint. Furthermore, dynamic assessment of the joint during the trialling process with accurate force feedback could also indicate the uniformity of force distribution across the joint. This will also inform on the peak forces in cases of prosthetic impingement. This force balancing is crucial to restoring the anatomy of the joint, to allow optimal function in terms of range of movement and pain reduction; it is also necessary to reduce the chances of dislocation, prosthetic impingement, and wear over time.

In the knee, the lack of quantitative force feedback during implant positioning to inform the surgeon on balancing and implant size choice has recently been addressed to an extent with the single-use VERASENSE sensor (Orthosensor Inc.) [21]. Surgeons are only able to balance the knee 50% of the time without VERASENSE, but once the technology is introduced into total knee replacements (TKRs), this rises to 92–100% of cases [22,23]. It has also been demonstrated that the requirement for manipulation under anaesthesia due to TKR complications is reduced by 3.2x if ligament balancing is achieved using VERASENSE during the operation [24]. This technology uses flat, rigid piezoelectric elements to provide force and positioning information during a TKR [25]. However, this cannot be readily adapted for the hip joint as it is curved and has much less space than the knee. Any solution for the hip requires components that are thin and flexible, but still capable of bearing heavy loads.

This lack of objective measurement of force distribution during the critical part of a hip replacement is a major unmet need, and addressing it has the potential to significantly reduce the number of hip revisions due to wear, dislocation, inadequate soft tissue balancing or prosthetic impingement.

To meet this need, we have developed a thin, flexible, biocompatible microfluidic force sensor that can be incorporated into the implant geometry during the trialling stage of performing a THR. We have also designed and fabricated a biomimetic trial insert to host an array of sensors in the acetabular part of the total hip replacement. We then designed and constructed a bespoke mechanical testing rig onto which the sensor-loaded trial insert could be mounted and a force could be applied via a femoral head at different angles. The distribution of force at the sensor locations could be recorded, thus providing a 3-dimensional representation of the forces in a cup as the surgeon inserts the femoral head and loads the hip at different angles. Importantly, we found that our experimental results were in agreement with simulated results from finite element modelling that was used to predict the forces measured by the individual sensors as a function of the loading angle. We designed the sensor to meet the requirements for force measurements in a THR, but the design can also be rapidly customised to target a range of biomedical force sensing applications. The sensors were fabricated via an additive manufacturing route, combining 3D and aerosol-jet printing.

2. Materials and methods

2.1. Finite element modelling of PDMS-based sensors in trial insert

COMSOL Multiphysics (COMSOL, United States) was used to produce a finite element model to simulate the force distribution

in the trial insert. This was therefore used to predict theoretical relative force readings between sensors located in different areas of the cup.

Ball and Socket model (Fig. 2): This was designed to model the ball and cup deformation, including the applied forces at different points in the cup when a certain force is applied by the head (the ball). The femoral head was made from a truncated sphere of alumina of radius 15 mm, using COMSOL's parameters for alumina (Young's Modulus E = 300 GPa, Poisson ratio ν = 0.22). The acetabular cup was modelled as a 1.5 mm-thick hemisphere with the same internal radius as the femoral head, made from high-density polyethylene (HDPE) because of its similarity to Formlabs' Durable Resin. The orientation of the head with respect to the cup axis (z-axis) was described by two angles θ_1 and θ_2 about orthogonal rotation axes (x- and y-axes, respectively). COMSOL's Structural Mechanics module was used to implement this. A *contact pair* was established between the head and cup's outer surface. The femoral head was set as the source and the cup was set as the destination, following recommendations from the COMSOL Structural Mechanics Module User's Guide [26]. The model was solved using the *penalty* method. The following boundary conditions were used: the ball and cup were defined as linear elastic; the ball outer surfaces and cup inner surfaces were free to move and deform; the cup outer surfaces were fixed; and the initial displacements of the ball and cup were set to zero. The ball was displaced down its axis (at angles of θ_1, θ_2 to the cup's z axis as previously described). Friction

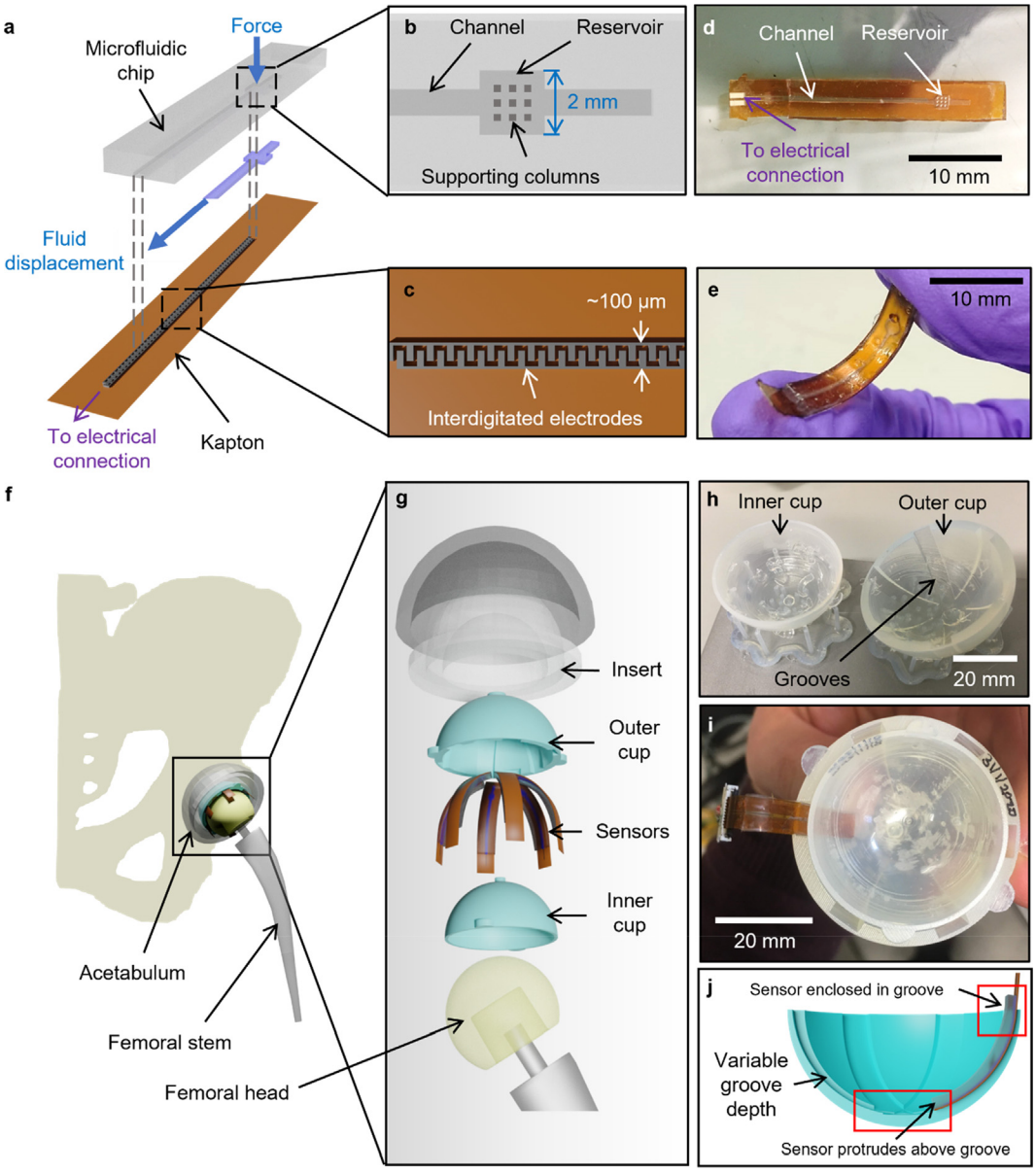

Fig. 1. Incorporating functionalised microfluidic sensors into the THR implant for force measurements. **(A)** The sensor is made of a soft elastomeric microfluidic chip layer and a Kapton substrate with aerosol-jet printed interdigitated electrodes. **(B)** The microfluidic chip layer contains an embedded microchannel with a fluid reservoir and optional supporting columns. **(C)** Interdigitated electrodes are aerosol-jet printed onto the Kapton substrate and consist of silver with an insulating polyimide coating. **(D)** Photograph of the sensor, highlighting the channel and reservoir. **(E)** Photograph of sensor, showing its flexibility. In this design, the reservoir has a round cross-section. **(F)** Standard geometry of a hip implant. The cup containing the sensors is incorporated into the polymer part of the implant's acetabular cup. **(G)** Our additions to the implant, during the trial stage, consist of an outer cup, the sensors which lie in the grooves of the outer cup, and the inner cup to act as an articulating surface with the femoral head. **(H)** Photograph of the SLA 3D printed inner and outer cup. **(I)** Photograph of a sensor located in a groove between the inner and outer cups. **(J)** Cross-section of the outer cup, showing how variable groove depth allows the channel to be shielded from force while the active sensing area (reservoir) is exposed.

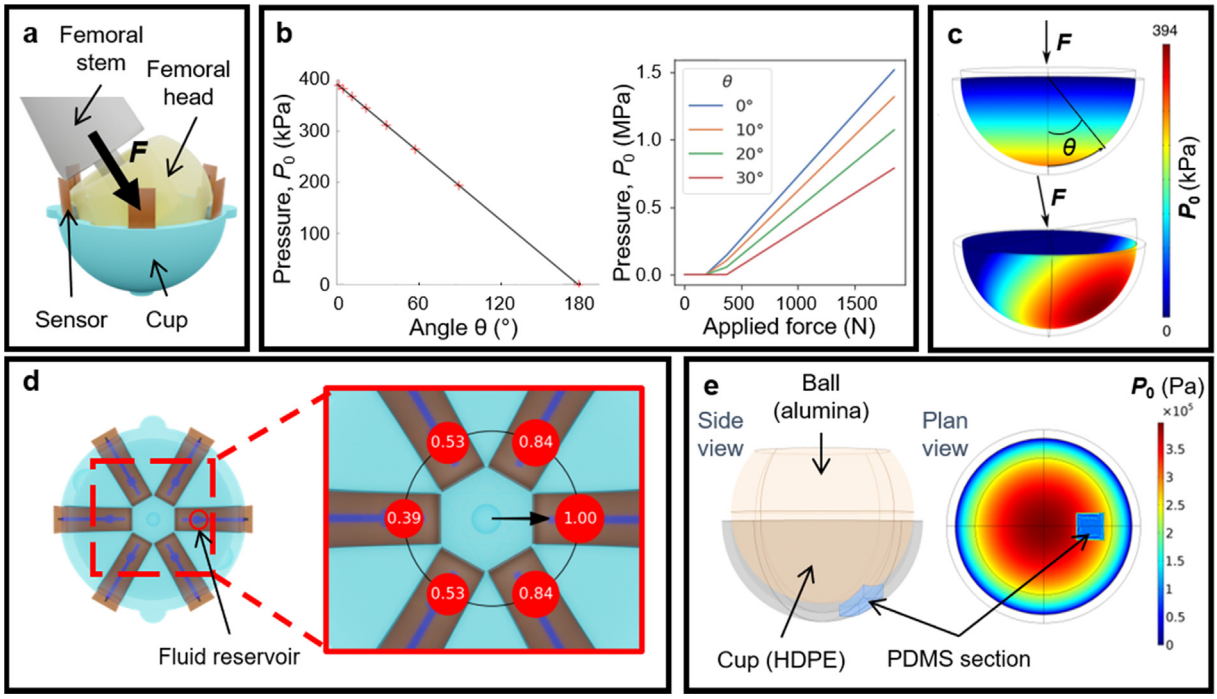

Fig. 2. Modelling the loading of sensors incorporated into implant acetabular component/cup geometry. (A) Schematic of angled loading; a force *F* is applied normal to a sensor's fluid reservoir, at 30° to the vertical. **(B),(C)** Finite element modelling simulations showing pressure P_0 in the cup as a function of applied force *F* and the cup angle between *F* and the cup normal, θ. **(D)** Plan view of the cup, showing an array of six sensors and their fluid reservoirs. The force is applied normal to one reservoir, at $\theta = 30°$, and the pressures shown are normalised by the pressure exerted on the reservoir closest to the contact point with the ball (femoral head). **(E)** Replacing a 5 mm^2 section of the cup with PDMS to show the effect of the cup shielding the sensors from the applied force.

between the head and cup was not included in this model, as only static loading was being simulated. The femoral head was meshed coarsely, from 2 mm elements. Both elements of the contact pair, the internal cup surface and femoral head surface were meshed as 0.6 mm and 1.1 mm respectively. The total force applied by the ball to the cup was calculated as a quadratic sum of the contact forces in the x, y, and z directions using a Global Evaluation. The contact pressures at each sensor were calculated from a Point Evaluation of the Von Mises stress at predefined points that correspond to the sensor reservoir locations.

The Supporting Information details the methods and results of finite element simulations to improve the sensor design by modelling electrode behaviour and the effect of reservoir dimensions and chip material on the sensor sensitivity.

2.2. Sensor fabrication

Flexible Resin microfluidic chip fabrication: The CAD file for the chip was custom-designed using Creo Parametric 6.0 (PTC, USA), and printed using on the Formlabs Form 3 stereolithography (SLA) 3D printer (Formlabs, USA) using the resin's smallest layer thickness of 50 µm. After printing, the chip was then washed in isopropanol (IPA) for 20 min in a sonicating bath before being transferred to the oven (FormCure, Formlabs, USA) for curing at 60 °C in 405 nm light for 10 min. The supports were then removed.

Interdigitated electrodes fabrication: 1–1.5 mL silver ink was produced by diluting Novacentrix Ag nanoparticles aerosol ink (JS-A221AE) 1:3 by volume with DI water. The ultrasonic atomiser (UA Max, Optomec, USA) in the aerosol-jet printer (AJP) (Optomec AJ200) was used with a tip size of 150 µm to print the electrodes on a 75 µm-thick Kapton (PI) film (RS Components Ltd., UK). Ink and sheath flow rates were 20 and 80 sccm respectively. The overall dimensions of the electrodes are 20 mm × 0.5 mm. Silver connecting pads were printed at the end of the electrodes, which fit a 2-pin flexible printed circuit (FPC) connector. The silver was then cured in the oven (Heratherm OGH60, Thermo Scientific, Germany) at 150 °C for 2 h. To print the insulating polyimide (PI) layer on top of the electrodes, a 15 mL PI ink made from a mix of poly(pyromellitic dianhydrideco- 4,4′-oxydianiline), amic acid solution (12.8 wt % in 80% NMP/20% aromatic hydrocarbon, Sigma-Aldrich, USA) and N-methyl-2-pyrrolidone (NMP) (Sigma-Aldrich, USA) at a 1:1 ratio by volume was used with the pneumatic atomiser and a tip size of 300 µm. The electrodes were covered with PI except for the connecting pads. To cure the polyimide, the electrodes were placed in the oven at 200 °C for 2 h. The Kapton was then cut into the correct shape and size.

Bonding the microfluidic chip to the electrode layer [27]**:** The adhesive layer connecting the microfluidic chip and Kapton electrode layer was made from laser-cut double-sided tape (RS Components Ltd., UK). The layer was designed in AutoCAD 2020 (Autodesk, USA), and then cut into the tape using a laser cutter (Epilog Zing 16, 30 W). Vector mode was used, with a resolution of 500 DPI and a frequency of 2500 Hz. The vector speed and power were 90% and 10% respectively. One side of the tape was then adhered to the microfluidic chip. The chip was then pressed onto the Kapton layer with the adhesive layer in between. The alignment between the chip and Kapton was then checked under an optical microscope. To minimise air bubbles between the chip and Kapton layers, a weight was put on top of the chip layer to press the two layers together.

Fluid injection: Fluid was injected into the channel to completely fill the reservoir up to the entrance to the channel. The injection hole is located adjacent to the reservoir but at the opposite end to the channel and was incorporated into the CAD file of the chip. The fluid, a 2:1 by volume glycerol-water mixture, was injected until it just filled the reservoir. The ratio was chosen to obtain a

balance between a low volatility and high dielectric constant. The hole was then sealed with the silicone sealant to prevent the fluid evaporating.

A list of components and materials used in finite element modelling and mechanical testing is provided in Table S1 (Supporting Information).

2.3. Experimental measurement of sensor response

Impedance Analyser: An ISX-3v2 impedance analyser (Sciospec, Germany) was used to measure the electrical impedance of the sensors. By using the simple circuit model for the sensor as a resistor in series with a capacitor, the impedance Z can be converted into a capacitance C using the equation $C = -(2\pi f \, \mathrm{Im}\{Z\})^{-1}$ where f is the measurement frequency in Hz. To determine the optimal f, frequency sweeps were conducted from 1 kHz to 1 MHz. Frequencies below 20 kHz were determined to have high noise, whereas higher frequencies had low impedance magnitudes. A compromise frequency of 500 kHz was selected for further measurements for a good signal-to-noise ratio. Three measurements were carried out at each applied force and averaged over three different loading cycles.

Linear Motor and Load Cell: A linear motor (LinMot, Switzerland) with a 20 N load cell (PCM Ltd., UK) was also used to test the sensors individually before incorporation into the implant geometry. It was found in practice that the load cell could read forces up to 40 N if a sufficient cooling system was put in place to prevent overheating.

Mechanical testing: Mayes 100 kN and Tinius Olsen 250 N mechanical machines were used to test the *in vitro* response of the sensors in the custom-made testing rig. To determine the maximum forces at which the sensor calibration broke down (for example, when the capacitance response plateaued), the femoral component was attached onto the load cell of the Mayes 100 kN servohydraulic testing machine, while the custom testing rig containing the acetabular component was screwed into the machine itself. For calibration, the testing rig was attached to the Tinius Olsen mechanical testing machine with a 250 N load cell. Details on the mechanical testing of the bulk microfluidic chip material are included in the Supporting Information.

3. Results

3.1. Design and operation of the microfluidic force sensor

Fig. 1a is a schematic of the sensor, whose design is based on the group's previous work [27]. The sensor consists of (1) a microfluidic chip (Fig. 1b) with an embedded microfluidic channel (20 mm × 0.75 mm × 0.3 mm) and fluid reservoir (2 mm × 2 mm × 0.3 mm), and (2) an electrode layer (Fig. 1c) comprising interdigitated silver electrodes on a flexible polyimide (PI, Kapton) substrate for mechanical support. The chip can be made using a silicone elastomer such as polydimethylsiloxane (PDMS) poured into a stereolithography (SLA) 3D printed mold, or directly SLA 3D printed by photo-curing an elastomeric resin (Flexible Resin, Formlabs). The channel is aligned above the electrodes and is open to air at the end opposite to the reservoir. The reservoir is the active sensing area. It has a square cross section, is filled with fluid by a syringe, and can contain internal columns for mechanical support. The interdigitated electrodes are made by aerosol-jet printing (AJP) silver nanoparticle ink onto Kapton and are protected by an aerosol-jet printed PI layer. The chip and electrode layer are bonded using laser-cut double-sided tape. Fig. 1d shows a photograph of the sensor, which has dimensions of approximately 30 mm × 5 mm × 1 mm and can be freely flexed (Fig. 1e) and incorporated into the THR UHMWPE insert without significant impact on sensor performance.

The operating principle is as follows [27]: when a force is applied to the fluid reservoir, the reservoir deforms and displaces fluid along the channel. The displaced fluid overlaps with the interdigitated electrodes, increasing the capacitance. The capacitance is calculated using the equation $C = \varepsilon_0 \varepsilon_r A/d$ where ε_r is the relative dielectric permittivity, A is the electrode area and d is the inter-electrode distance. The fluid determines the value of ε_r. On releasing the force, the fluid returns to the reservoir.

The sensors are durable, with measurements reproduced over more than 2,000 loading cycles in a mechanical testing rig [27]. For each sensor, the force-capacitance relationship is calibrated by applying a known force and measuring the corresponding impedance using an impedance analyser, which is converted to a capacitance. For the present application, an array of sensors is embedded into the UHMWPE component.

Importantly, these sensors can be easily and rapidly customised to suit a range of applications by changing the reservoir and channel size, electrode size and spacing, chip material and device size. While this sensor has been developed for hip applications, we have fabricated sensors with alternative designs, including a sensor incorporating three sensing elements intended for the knee joint both for the TKR and unicompartmental applications.

3.2. Incorporation of sensors into implant

To test the sensor's performance in the hip, a biomimetic trial insert (Fig. 1f) was designed using Creo Parametric and produced by SLA 3D printing. The insert (Fig. 1g,h) consists of an 'outer cup', which contains grooves to fit sensors; and an 'inner cup', which has a smooth inner surface to act as an articulating surface with the femoral head, and pegs to secure it in the outer cup. It was decided to incorporate six sensors into the trial insert to provide a balance between providing many sensing regions and mechanical stability when loading the sensors. The sensors were incorporated into the grooves (Fig. 1i) such that the reservoirs were at 30° to the cup axis. In this study, the outer cup has an external diameter of 43 mm and an internal diameter of 41 mm, but this can be adapted to suit femoral heads of different sizes. Typically, the femoral head has a diameter between 28 and 40 mm [1]. The groove depth is deliberately reduced going from the outside of the cup towards the centre (Fig. 1j). This gives the effect of raising the reservoirs out of the grooves, such that an applied force is concentrated on the fluid reservoirs (the active sensing area) while shielding the channel.

Formlabs' Durable Resin was used as the cup material – the resin has similar mechanical properties to the UHMWPE used in the acetabular insert of real hip implants (see Supporting Information Fig. S6 for mechanical characterisation).

3.3. Finite element modelling of sensors within implant geometry

Finite element models were produced to: 1) improve the sensor design by modelling electrode behaviour and the effect of reservoir dimensions and chip material on the sensitivity, and 2) obtain a theoretical force distribution in the trial insert upon application of an external force over a range of magnitudes and orientations relative to the cup, similar to a surgeon inserting and testing the implant during THR. The corresponding methods and results of the former are presented in the Supporting Information; here, we focus on simulating the sensors in the implant trial insert geometry.

A finite element model was created to simulate the interaction between the ball-like femoral head and socket i.e. the cup or acetabular component (Fig. 2), including the simulated forces at

different points in the cup when a certain force is applied by the head. This model determines the theoretical force that each sensor should be reading, to compare to the actual response of the sensors in practice. Fig. 2a shows a schematic of the loading setup in the model – the ball-like femoral head applies a force F to the cup-like acetabular part of the implant.

Fig. 2b shows how the pressure P_0 at a point on the internal surface of the cup varies with angle θ (in degrees) and magnitude F of the applied force. P_0 increases with applied load, and decreases linearly with angle θ from the force axis, resulting in the equation $P_0 = P_{max}(1 - \theta^2/\pi^2)$ where the pressure is at a maximum (P_{max}) at an angle of 0°. This expression agrees with the paraboloidal theory of contact between a sphere and a cup as established by Calonius and Saikko [28]. Fig. 2c shows a heat map of P_0 at θ = 0° and 30°. The model is used to carry out proof-of-concept simulations of the balance within the joint geometry. Fig. 2d shows the relative pressures exerted on the sensor reservoirs when a force is applied directly onto one of the reservoirs, at θ = 30°. This model will be used as a guide in the calibration of sensors in the hip implant geometry.

To determine the effect of incorporating sensors into the cup grooves, a 5 mm × 5 mm square section of the HDPE cup was replaced with PDMS (Fig. 2e) at a cup angle θ = 30°, to represent a sensor embedded into the cup. The pressure P_0 was approximately 3.6 times smaller on the PDMS section (P_0 = 96 kPa) than on an HDPE section at the same cup angle (P_0 = 344 kPa), which represents a section of the cup made from the cup material with no embedded sensor. This indicates that the stiffer cup material is shielding the sensors from the applied force with the sensor-cup combination acting like a composite material, allowing the sensors to remain intact at higher applied forces. Fig. 2e also indicates that the shielding effect does not significantly change the forces in the areas of the cup surrounding the PDMS square. This analysis was also compatible with the observation that the maximum operating applied force was considerably higher in this cup geometry, with a sensitivity value of approximately 0.03 pF N^{-1} – compared to 0.06 pF N^{-1} when calibrating the sensors when not housed in the cup (see Fig. S2 of the Supporting Information).

3.4. Mechanical testing of sensors within implant geometry validates simulation results

To validate the simulation results, we designed a custom mechanical testing rig (Fig. 3a) to experimentally apply an external force from the head to the cup component in the hip implant. The rig consists of a polycarbonate (PC) support that houses a rotating brass stage. The stage has been machined to house the outer cup (Fig. 1g-i), which is held in place by semi-circular pegs. The sensors are inserted into the grooves between the inner and outer cups. The femoral head is attached to the moving component of a mechanical testing machine and is lowered into the cup to apply the desired forces. This rig was used with two mechanical testing machines: the Tinius Olsen 250 N and the Mayes 100 kN for lower and higher forces respectively. The stage can rotate and be locked in position to load the cup at angles of up to θ = 30° to the cup normal in approximately 5° increments.

Fig. 3b demonstrates the effect of loading and unloading one sensor from applied force F = 0 N to a maximum force F_{max}, which varied from 100 to 1800 N, over 14 loading cycles. During each cycle, the force was applied linearly from 0 N to F_{max}, held at F_{max} for 10 s, then unloaded with the same linear relationship. A clear increase in capacitance values can be seen as F_{max} increases to 400 N, above which the capacitance response starts to plateau, which would complicate calibration. The maximum capacitance change ΔC also decreases with increase in F_{max} above 700 N, indicating that fluid may be lost from the sensor. This is an appropriate force range for applications in hip surgery, but it can be increased by modifying the sensor design, for example by changing the channel and reservoir dimensions.

Fig. 3c shows the loading and unloading of six sensors incorporated into the cup, with F_{max} = 20 N and θ = 0°. The sensor reservoirs, the active sensing components, were located at 30° to the cup centre. The cup was loaded to 20 N, the force was held at approximately 20 N for 20 s, then the cup was unloaded to 0 N. The sensors vary in response, which could indicate imbalance in the loading setup. Fig. 3d repeats this experiment for a cup angle of θ = 30°, showing the effect of the new cup orientation. The sensors with reservoirs closer to the axis of applied forces demonstrated a greater increase in capacitance. These experiments were repeated over 20 loading cycles without significant change in device performance, but the individual sensors can last up to at least 100 loading cycles without failure (see Supporting Information Fig. S14). The data in Fig. 3c and 3d also show a delay of a few seconds between applying the force and the sensors' response, which may be due to force being applied too quickly relative to the fluid's relaxation time.

Fig. 4 shows the calibration when a series of load cycles were applied, with the maximum force reached increasing from 50 N up to 200 N and decreasing back to 50 N. Fig. 4a demonstrates that the sensors can be loaded up to 200 N and then back to 50 N without a significant change in performance. Fig. 4b is a plot of the change in capacitance with force, calculated from capacitance-time and force-time data. The loading curves all show a similar sensitivity of 0.03 pF N^{-1}, but the unloading curves show large hysteresis. This hysteresis is only present when calibrating the sensors inside the curved trial insert geometry – it is not present when the sensors are calibrated using the linear motor, when the sensors are flat [27] (also see Supporting Information Fig. S2). The hysteresis is consistent between cycles, so does not significantly affect the calibration. It may arise from the fluid wetting the channel's internal surface, causing a time delay as the liquid returns to the reservoir. This hysteresis could be reduced by choosing a liquid that has less favourable interactions with the channel. Additional calibration, including varying the cup and stage angle and determining the consistency of samples, can be found in the Supporting Information Figs. S15 and S16.

In this loading setup, the gradient of the capacitance-force calibration curve was lower – approximately 0.03 pF N^{-1} compared to 0.06 pF N^{-1} when calibrated outside of the cup [27]. It is therefore likely that the cup is acting to shield the sensors from these forces as previously indicated by the modelling results. This agrees with the observation that the maximum operating applied force for the sensors was considerably higher in this trial insert than when the sensors were calibrated on their own.

We have also characterised how modifications to both the chip design and material may affect device performance; such data (experimental and computational) is in the Supporting Information.

4. Discussion

This paper summarises the design, production and characterisation of a next-generation hip implant technology that contains microfluidic force sensors, designed to replace part of the trial insert during surgery while the surgeon dynamically assesses the THR positioning, soft tissue tensioning, size and prosthetic impingement. This will provide the surgeon with quantitative data on the interfacial forces between the implant's femoral head and insert during the THR, so that imbalance and improper positioning can be detected and corrected, decreasing the rate of implant failure. This is crucial, as surgeon experience is linked to fewer compli-

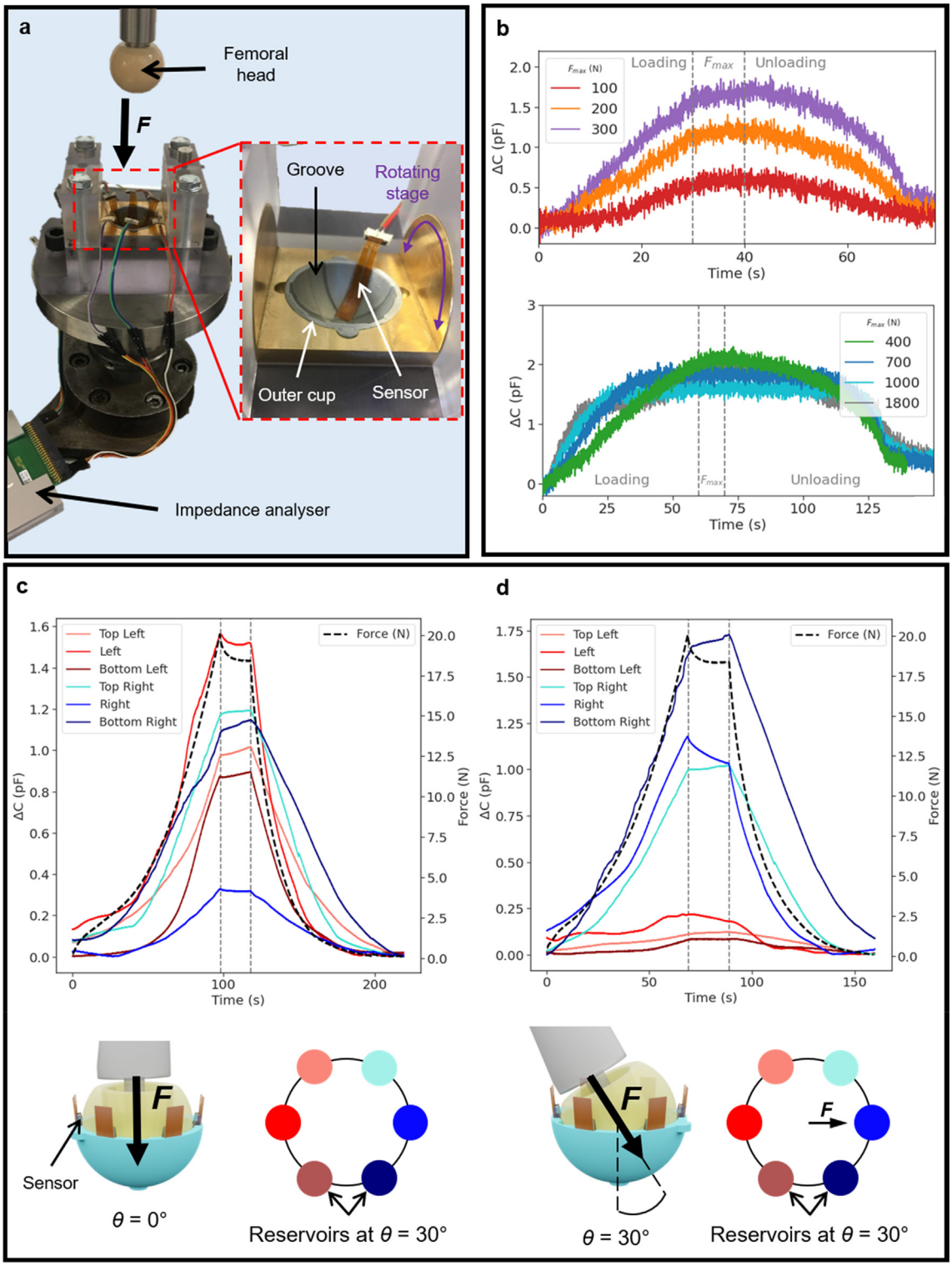

Fig. 3. Mechanical testing of sensors in trial hip implant geometry. (A) Custom-built testing rig for use with the Mayes 100 kN Universal servohydraulic test machine. [Inset] The central stage rotates to load the insert cups at angles of up to 30°. **(B)** Loading one sensor in the cup geometry up to a maximum applied force, F_{max}. [Top] There is a clear force-capacitance relationship between F_{max} = 100 N and 300 N. [Bottom] In order to reach higher forces, a different machine was used – therefore, the measurement duration is longer. The sensor is operational up to at least 400 N, above which the response begins to plateau. **(C)** Loading six sensors in the trial insert up to F_{max} = 20 N at a cup angle θ = 0°. The coloured lines and dots indicate different sensors. **(D)** Loading six sensors in the trial insert up to F_{max} = 20 N. The force is applied normal to a sensor's reservoir, at a cup angle θ = 30°.

cations during surgery and better patient satisfaction post-surgery [29,30].

Furthermore, it is well-documented that specialised hip surgeons are less likely to have complications as compared with general orthopaedic surgeons, and patients operated on by orthopaedic trainees report less satisfaction than surgeons with greater than 15 years of experience according to data from the Swedish Joint Registry [29–31]. The objective force feedback our

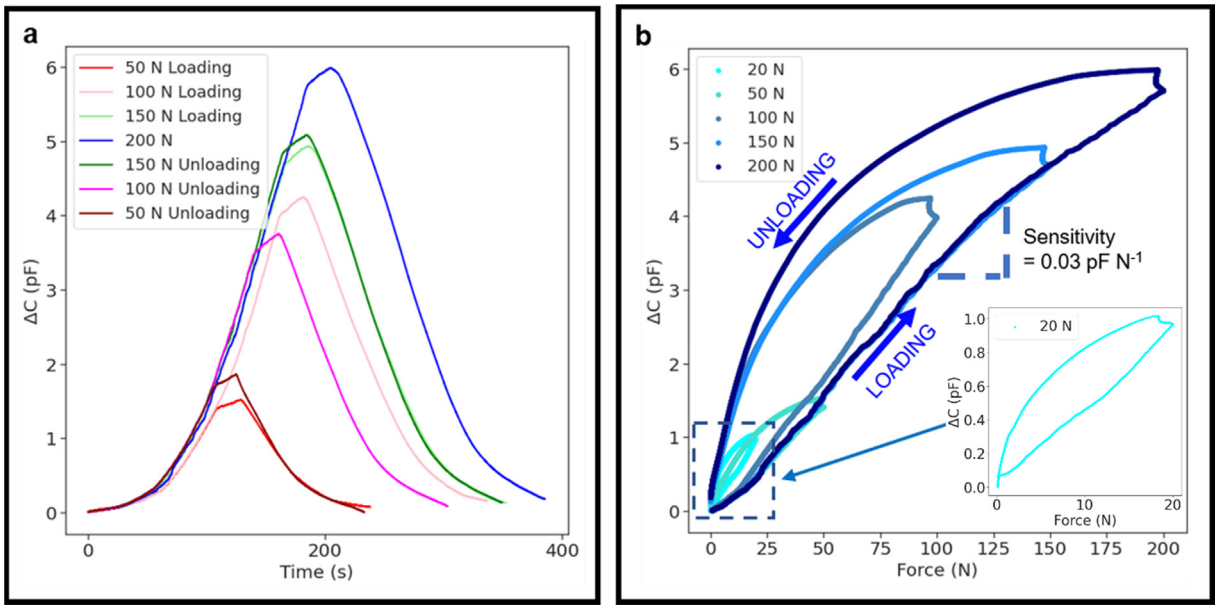

Fig. 4. Sensor calibration and hysteresis behaviour in trial insert. (A) A series of loading curves showing change in capacitance over time, increasing F_{max} from 50 N to 200 N then decreasing it to 50 N. The experiments were performed in the order shown in the legend (top to bottom). **(B)** Force-capacitance calibration curves for the loading curves in **(A)**. The sensors exhibit significant hysteresis, with non-linear unloading curves indicating wetting of the channels by the fluid. This hysteresis is consistent between loading cycles, and therefore does not significantly affect calibration.

technology provides has the potential to augment training and reduce learning curves in hip replacement surgery by allowing trainee surgeons to receive visual and haptic feedback of the accuracy of implant positioning during the trialling process. Therefore, quantitative force data could be a useful tool to both improve the technique of experienced surgeons and as a training tool for non-specialists to perform the same surgery with the same outcomes.

Although accurate implant placement has now been addressed to an extent with navigation or robotic assisted techniques, difficulties with inappropriate soft tissue balance and prosthetic impingement remain unaddressed, leading to poor functional outcomes and accelerated wear [32]. Furthermore, they require a significant amount of investment and are not available for routine use in most hospitals worldwide [33].

Many different existing sensing mechanisms could potentially meet the clinical need for quantitative force sensing, including capacitive, resistive, piezoresistive, optical, triboelectric, magnetic, passive resonator and FET-based sensors [34]. Capacitive sensors have limited spatial resolution compared to resistive ones, but have a higher reliability [35–40]. Flexible microfluidic force sensors have been made previously for tactile and haptic sensing [41–43], but could not reach the high forces required in this application. Some devices can reach higher resolutions, but each sensing element requires a large support system featuring electrical connections [44] or power supplies.

Here, we have developed a capacitive microfluidic force sensor that is conformable and functional at the forces used in hip surgery. The force sensors were incorporated into 3D printed trial inserts which were subjected to loading forces at different angles through a femoral head in a custom-made mechanical testing rig that was designed to mimic loading conditions during surgery. The force distributions acquired from the sensors under different loading conditions were in agreement with those acquired through finite element modelling of the sensor-loaded inserts. The sensors were therefore experimentally and computationally validated for application in THR. Whilst prosthetic impingement and soft tissue balance are key in assessing the stability of a THR intra-operatively, these conditions were not simulated in the lab with the current experiments. The next phase of our experiments includes cadaveric testing which will involve both these simulations in the cadaveric setting.

Mechanical characterisation has demonstrated that the sensors can measure forces up to at least 400 N, which meets the expected requirements for the force range applied by the surgeon during THR [34,45]. This is orders of magnitude above the capability of similar microfluidic or flexible pressure sensors in the literature [46–48]. In the current design, the response beyond 400 N is saturated, but this can be easily adjusted by changing the chip and electrode geometry, the material stiffness and the trial insert design. Our results indicate some hysteresis in the loading and unloading cycles, which could have an effect on long-term performance, depending on the underlying mechanism. For example, viscoelastic relaxation of the solid microfluidic chip would give rise to loading frequency dependent hysteresis, but this would not depend on the number of cycles. However, if the hysteresis behaviour is due to absorption of fluid by the electrodes over time, then this would require the sensors to be calibrated prior to each use. Mechanical testing also revealed that there is no loss of sensor functionality when curved, and they can be repeatedly loaded at these high forces. The device currently incorporates six sensors, but by improving the chip and electrode design, including wireless sensing, more sensing elements can be incorporated.

The sensors and trial implant provide minimal modification to the insert itself during surgery. Existing devices in the literature either modify the implant geometry [25,39,49], which has been deemed expensive and technically challenging [34], disturb the contact zone between the femoral head and acetabular cup [48,50], or are implanted away from the contact area and therefore do not directly measure contact forces [51].

Furthermore, the sensors and cups can be rapidly produced by a combination of aerosol-jet printing and stereolithography 3D printing over a few hours, which is a significant improvement over traditional soft lithography methods that can be several times more expensive and time-consuming [52]. Therefore, while these sensors have been demonstrated to work in the ball and cup hip joint geometry, there is scope to adapt the sensor design to work

in other areas of the body, including the knee, in the patellofemoral joint and in medial and lateral compartmental replacement, as well as in the spine, shoulder and ankle.

While these sensors have advantages of flexibility, greater force range and ease of manufacture, they must also be sensitive enough to detect imbalance. Studies using sensor-guided technology in the knee [53,54] that used two force-sensing components defined that the implant is 'balanced' if the two sensing components registered a difference of 67 N, which our sensors can easily distinguish. In the future, *in vivo* testing will be carried out to demonstrate the technology's usefulness in desired settings. Biocompatibility tests will be performed to determine the host's response to the sensors. Cadaveric testing will test the usage of the sensor-loaded trial insert. The sensors have been tested and shown to work at ambient temperatures (10–50 °C).

In summary, we present a thin, flexible, and robust capacitive microfluidic force sensor, that can be fabricated quickly and cheaply using additive manufacturing. A custom-made mechanical testing rig was designed, produced, and used to demonstrate that the sensors can be loaded up to the forces typically applied by the surgeon during THR. The results obtained from the mechanical loading experiments were in agreement with finite element simulations under similar conditions. Due to the sensor design's customisability and adaptability, in the future these sensors could be used in a range of different applications where force monitoring and balancing is essential.

Funding

LI acknowledges support from an EPSRC Doctoral Training Partnership studentship (EP/R513180/1).

TW acknowledges support from an EPSRC Doctoral Training Partnership studentship (EP/T517847/1).

SK-N is grateful for support from ERC Starting Grant (Grant No. ERC-2014-STG-639526, NANOGEN).

SK-N and QJ acknowledge support from the Centre of Advanced Materials for Integrated Energy Systems "CAM-IES" grant EP/P007767/1.

JC was supported by a Wellcome Trust Institutional Strategic Support Award to the University of Exeter (204909/Z/16/Z); for the purpose of Open Access, the author has applied a CC BY public copyright license to any Author Accepted Manuscript version arising from this submission.

Data and materials availability

All data required for interpreting the manuscript are available in the main text or the supplementary materials. Supporting data for this paper is available at the DSpace@Cambridge data repository (https://doi.org/10.17863/CAM.84650).

CRediT authorship contribution statement

Liam Ives: Conceptualization, Methodology, Investigation, Visualization, Writing – original draft, Writing – review & editing. **Alizée Pace:** Methodology, Investigation, Writing – review & editing. **Fabian Bor:** Methodology, Investigation, Writing – review & editing. **Qingshen Jing:** Methodology, Investigation, Writing – review & editing. **Tom Wade:** Methodology, Investigation, Visualization, Writing – review & editing. **Jehangir Cama:** Conceptualization, Writing – review & editing. **Vikas Khanduja:** Conceptualization, Writing – review & editing. **Sohini Kar-Narayan:** Conceptualization, Methodology, Supervision, Writing – review & editing.

Declaration of Competing Interest

LI, QJ, VK, JC, and SK-N are named inventors on a patent application by Cambridge Enterprise that covers the technology described in this study. SK-N, VK and JC are co-founders and directors of Artio-Sense Ltd., incorporated to translate and commercialise aspects of this work. VK is Consultant for Arthrex and Smith and Nephew Limited. All other authors declare they have no competing interests.

Appendix A. Supplementary material

Supplementary data to this article can be found online at https://doi.org/10.1016/j.matdes.2022.110747.

References

[1] P. Howard et al., National Joint Registry | 17th Annual Report, 2020. www.njrcentre.org.uk (accessed December 2, 2020).
[2] S. Tanna et al., Background Paper 6.12 Osteoarthritis, 2013.
[3] R.D. Crowninshield, A.G. Rosenberg, S.M. Sporer, Changing demographics of patients with total joint replacement, Clin. Orthop. Relat. Res. 443 (2006) 266–272, https://doi.org/10.1097/01.blo.0000188066.01833.4f.
[4] J.T. Evans, J.P. Evans, R.W. Walker, A.W. Blom, M.R. Whitehouse, A. Sayers, How long does a hip replacement last? A systematic review and meta-analysis of case series and national registry reports with more than 15 years of follow-up, The Lancet. 393 (10172) (2019) 647–654, https://doi.org/10.1016/S0140-6736(18)31665-9.
[5] R.L. Barrack, Economics of revision total hip arthroplasty, Curr. Orthop. (1995) 209–214, https://doi.org/10.1016/j.cuor.2006.02.007.
[6] R.L. Barrack, J. Sawhney, J. Hsu, R.H. Cofield, Cost Analysis of Revision Total Hip Arthroplasty: A 5-Year Followup Study, Clin. Orthop. Relat. Res. 369 (1999) 175–178.
[7] M.A. Ritter, K.D. Carr, E.M. Keating, P.M. Faris, D.L. Bankoff, P.H. Ireland, Revision total joint arthroplasty: Does medicare reimbursement justify time spent?, Orthopedics 9 (1) (1994) 115, https://doi.org/10.1016/0883-5403(94)90185-6.
[8] C. Lavernia, A. Tsao, D. Hungerford, Revision and primary hip and knee arthroplasty: A cost analysis, Clin. Orthop. Relat. Res. 8 (1) (1993) 103–104.
[9] R.L. Barrack, G.J. Hoffman, W.V. Tejeiro, L.J. Carpenter, Surgeon work input and risk in primary versus revision total joint arthroplasty, J. Arthroplasty 10 (3) (1995) 281–286, https://doi.org/10.1016/S0883-5403(05)80175-5.
[10] J.F. Crowe, T.P. Sculco, B. Kahn, Revision Total Hip Arthroplasty: Hospital Cost and Reimbursement Analysis, Clin. Orthop. Relat. Res. 413 (2003) 175–182, https://doi.org/10.1097/01.blo.0000072469.32680.b6.
[11] P. Sadoghi, M. Liebensteiner, M. Agreiter, A. Leithner, N. Böhler, G. Labek, Revision surgery after total joint arthroplasty: A complication-based analysis using worldwide arthroplasty registers, J. Arthroplasty 28 (8) (2013) 1329–1332, https://doi.org/10.1016/j.arth.2013.01.012.
[12] G.E. Lewinnek, J.L. Lewis, R. Tarr, C.L. Compere, J.R. Zimmerman, Dislocations after total hip-replacement arthroplasties, J Bone Joint Surg Am. 60 (2) (1978) 217–220.
[13] K.J. Bozic et al., The epidemiology of revision total knee arthroplasty in the united states, in: Clinical Orthopaedics and Related Research, Springer New York LLC, 2010: pp. 45–51. https://doi.org/10.1007/s11999-009-0945-0.
[14] A.M. DiGioia, B. Jaramaz, M. Blackwell, D.A. Simon, F. Morgan, J.E. Moody, C. Nikou, B.D. Colgan, C.A. Aston, R.S. Labarca, E. Kischell, T. Kanade, Image guided navigation system to measure intraoperatively acetabular implant alignment, Clin. Orthop. Relat. Res. 355 (1998) 8–22, https://doi.org/10.1097/00003086-199810000-00003.
[15] M.C. Callanan et al., Risk factors for cup malpositioning: Quality improvement through a joint registry at a tertiary hospital, Clin. Orthop. Relat. Res. 469 (2011) 319–329, https://doi.org/10.1007/s11999-010-1487-1.
[16] T. Yamaguchi, M. Naito, I. Asayama, T. Ishiko, Total hip arthroplasty: the relationship between posterolateral reconstruction, abductor muscle strength, and femoral offset, J Orthop Surg (Hong Kong). 12 (2) (2004) 164–167, https://doi.org/10.1177/230949900401200205.
[17] B.J. McGrory, B.F. Morrey, T.D. Cahalan, K.N. An, M.E. Cabanela, Effect of femoral offset on range of motion and abductor muscle strength after total hip arthroplasty, J. Bone Joint Surg - Series B 77-B (6) (1995) 865–869.
[18] I. Asayama, M. Naito, M. Fujisawa, T. Kambe, Relationship between radiographic measurements of reconstructed hip joint position and the Trendelenburg sign, J. Arthroplasty 17 (6) (2002) 747–751, https://doi.org/10.1054/arth.2002.33552.
[19] I. Asayama, S. Chamnongkich, K.J. Simpson, T.L. Kinsey, O.M. Mahoney, Reconstructed hip joint position and abductor muscle strength after total hip arthroplasty, J. Arthroplasty 20 (4) (2005) 414–420, https://doi.org/10.1016/j.arth.2004.01.016.
[20] D.P. Sakalkale, P.F. Sharkey, K. Eng, W.J. Hozack, R.H. Rothman, Effect of femoral component offset on polyethylene wear in total hip arthroplasty, Clin. Orthop. Relat. Res. 388 (2001) 125–134, https://doi.org/10.1097/00003086-200107000-00019.

[21] S. Almouahed, M. Gouriou, C. Hamitouche, E. Stindel, C. Roux, Design and evaluation of instrumented smart knee implant, IEEE Trans. Biomed. Eng. 58 (4) (2011) 971–982, https://doi.org/10.1109/TBME.2010.2058806.
[22] M.A. Gharaibeh, D.B. Chen, S.J. MacDessi, Soft tissue balancing in total knee arthroplasty using sensor-guided assessment: is there a learning curve?, ANZ J Surg 88 (5) (2018) 497–501.
[23] K.-J. Cho et al., Objective quantification of ligament balancing using VERASENSE in measured resection and modified gap balance total knee arthroplasty, BMC Musculoskelet Disord. 19 (2018) 1–11.
[24] J.A. Geller, A. Lakra, T. Murtaugh, The Use of Electronic Sensor Device to Augment Ligament Balancing Leads to a Lower Rate of Arthrofibrosis After Total Knee Arthroplasty, J. Arthroplasty 32 (5) (2017) 1502–1504.
[25] O. Müller, W.J. Parak, M.G. Wiedemann, F. Martini, Three-dimensional measurements of the pressure distribution in artificial joints with a capacitive sensor array, J. Biomech. 37 (10) (2004) 1623–1625, https://doi.org/10.1016/j.jbiomech.2004.01.024.
[26] COMSOL, The Structural Mechanics Module User's Guide, 2018. www.comsol.com/blogs (accessed June 11, 2020).
[27] Q. Jing, A. Pace, L. Ives, A. Husmann, N. Ćatić, V. Khanduja, J. Cama, S. Kar-Narayan, Aerosol-jet-printed, conformable microfluidic force sensors, Cell Rep. Phys. Sci. 2 (4) (2021) 100386, https://doi.org/10.1016/j.xcrp.2021.100386.
[28] O. Calonius et al., Analysis of Relative Motion between Femoral Head and Acetabular Cup and Advances in Computation of the Wear Factor for the Prosthetic Hip Joint, Acta Polytech. 43 (2003) 43–54. https://doi.org/10.14311/454.
[29] H. Malchau et al., Prognosis of Total Hip Replacement: Update and Validation of Results from the Swedish National Hip Arthroplasty Registry 1979-1998, American Academy of Orthopaedic Surgeons, 2000. www.jru.orthop.gu.se (accessed April 9, 2020).
[30] G. Green, M. Khan, F.S. Haddad, (i) Why do total hip replacements fail?, Orthopaed Trauma 29 (2) (2015) 79–85.
[31] P. Jolbäck, O. Rolfson, M. Mohaddes, S. Nemes, J. Kärrholm, G. Garellick, H. Lindahl, Does surgeon experience affect patient-reported outcomes 1 year after primary total hip arthroplasty?: A register-based study of 6,713 cases in western Sweden, Acta Orthopaedica. 89 (3) (2018) 265–271, https://doi.org/10.1080/17453674.2018.1444300.
[32] Z. Liu, Y. Gao, L. Cai, Imageless navigation versus traditional method in total hip arthroplasty: A meta-analysis, Int. J. Surg. 21 (2015) 122–127, https://doi.org/10.1016/j.ijsu.2015.07.707.
[33] P. Kouyoumdjian, J. Mansour, C. Assi, J. Caton, S. Lustig, R. Coulomb, Current concepts in robotic total hip arthroplasty, SICOT J. 6 (2020) 45, https://doi.org/10.1051/sicotj/2020041.
[34] E.H. Ledet et al., Smart implants in orthopedic surgery, improving patient outcomes: a review, Innovat. Entrepren. Health 5 (2018) 41–51, https://doi.org/10.2147/ieh.s133518.
[35] B.S. Cook, J.R. Cooper, M.M. Tentzeris, An inkjet-printed microfluidic RFID-enabled platform for wireless lab-on-chip applications, IEEE Trans. Microw. Theory Tech. 61 (12) (2013) 4714–4723, https://doi.org/10.1109/TMTT.2013.2287478.
[36] M. Raibert, An all digital VLSI tactile array sensor, in: Proceedings - IEEE International Conference on Robotics and Automation, Institute of Electrical and Electronics Engineers Inc., 1984: pp. 314–319. https://doi.org/10.1109/ROBOT.1984.1087183.
[37] Y. Otake, N. Suzuki, A. Hattori, H. Miki, M. Yamamura, K. Yonenobu, T. Ochi, N. Sugano, System for intraoperative evaluation of soft-tissue-generated forces during total hip arthroplasty by measurement of the pressure distribution in artificial joints, Comput. Aided Surg. 12 (1) (2007) 53–59, https://doi.org/10.3109/10929080701210881.
[38] D. Forchelet, M. Simoncini, A. Arami, A. Bertsch, E. Meurville, K. Aminian, P. Ryser, P. Renaud, Enclosed Electronic System for Force Measurements in Knee Implants, Sensors. 14 (8) (2014) 15009–15021, https://doi.org/10.3390/s140815009.
[39] C. Micolini et al., Conductive polymer sensor arrays for smart orthopaedic implants, in: Nanosensors, Biosensors, in: Info-Tech Sensors and 3D Systems 2017, 2017, p. 101670D, https://doi.org/10.1117/12.2260404.
[40] E.J. Curry, K. Ke, M.T. Chorsi, K.S. Wrobel, A.N. Miller, A. Patel, I. Kim, J. Feng, L. Yue, Q. Wu, C.-L. Kuo, K.-H. Lo, C.T. Laurencin, H. Ilies, P.K. Purohit, T.D. Nguyen, Biodegradable Piezoelectric Force Sensor, PNAS 115 (5) (2018) 909–914, https://doi.org/10.1073/pnas.1710874115.
[41] E. Ledet et al., Wireless Implantable Sensors with No Electrical Connections Enable the Next Generation of Smart Orthopaedic Implants, Bone Zone. (2012) 82–84. https://www.bonezonepub.com/449-wireless-implantable-sensors-with-no-electrical-connections-enable-the-next-generation-of-smart-orthopaedic-implants (accessed April 1, 2020).
[42] R. Wachs et al., Elementary Implantable Force Sensor For Smart Orthopaedic Implants accessed April 1, 2020, Adv. Biosensors Bioelectron. (ABB) 2 (2013) 57–64. https://digitalcommons.unl.edu/biosysengfacpub/504.
[43] S. Cheng, Z. Wu, A microfluidic, reversibly stretchable, large-area wireless strain sensor, Adv. Funct. Mater. 21 (12) (2011) 2282–2290, https://doi.org/10.1002/adfm.201002508.
[44] D. Panescu, Emerging technologies: Wireless communication systems for implantable medical devices, IEEE Eng. Med. Biol. Mag. 27 (2) (2008) 96–101, https://doi.org/10.1109/EMB.2008.915488.
[45] P.J. Sell, Instrumented implants in orthopaedics, J. Biomed. Eng. 11 (2) (1989) 111–112, https://doi.org/10.1016/0141-5425(89)90118-0.
[46] Q. Shi, H. Wang, T. Wang, C. Lee, Self-powered liquid triboelectric microfluidic sensor for pressure sensing and finger motion monitoring applications, Nano Energy 30 (2016) 450–459, https://doi.org/10.1016/j.nanoen.2016.10.046.
[47] R.D. Ponce Wong, J.D. Posner, V.J. Santos, Flexible microfluidic normal force sensor skin for tactile feedback, Sensors Actuat. A: Phys. 179 (2012) 62–69, https://doi.org/10.1016/j.sna.2012.03.023.
[48] W.-Y. Tseng et al., A slow-adapting microfluidic-based tactile sensor, J. Micromech. Microeng. 19 (8) (2009) 085002, https://doi.org/10.1088/0960-1317/19/8/085002.
[49] T.G. McPoil et al., A comparison of two in-shoe plantar pressupe measurement systems, Lower Extremity. 2 (1995) 95–103. https://www.researchgate.net/publication/236975064_A_comparison_of_two_in-shoe_plantar_pressure_measurement_systems.
[50] Y.L. Park et al., Smart pneumatic artificial muscle actuator with embedded microfluidic sensing, in: SENSORS, 2013 IEEE, IEEE, 2013: pp. 1–4. https://doi.org/10.1109/ICSENS.2013.6688298.
[51] F. Graichen, G. Bergmann, Four-channel telemetry system for in vivo measurement of hip joint forces, J. Biomed. Eng. 13 (5) (1991) 370–374, https://doi.org/10.1016/0141-5425(91)90016-Z.
[52] N. Ćatić et al., Aerosol-jet printing facilitates the rapid prototyping of microfluidic devices with versatile geometries and precise channel functionalization, Appl. Mater. Today 19 (2020) 100618, https://doi.org/10.3390/w9120928.
[53] K.A. Gustke, G.J. Golladay, M.W. Roche, L.C. Elson, C.R. Anderson, Primary TKA Patients with Quantifiably Balanced Soft-Tissue Achieve Significant Clinical Gains Sooner than Unbalanced Patients, Adv. Orthop. 2014 (2014) 1–6, https://doi.org/10.1155/2014/628695.
[54] S. MacDessi et al., Accuracy of Manual Surgeon-Defined Assessment of Soft Tissue Balance in TKA In Comparison to Sensor-Guided Measures and its Effect on Final Balance, Orthop. J. Sports Med. 5 (2017) 2325967117S0016. https://doi.org/10.1177/2325967117s00161.